ACS APPLIED MATERIALS & INTERFACES

Research Article

www.acsami.org

Highly Stretchable, Hysteresis-Free Ionic Liquid-Based Strain Sensor for Precise Human Motion Monitoring

Dong Yun Choi,[†,¶] Min Hyeong Kim,[†,‡,¶] Yong Suk Oh,[§] Soo-Ho Jung,[†] Jae Hee Jung,[∥] Hyung Jin Sung,[§] Hyung Woo Lee,[*,‡] and Hye Moon Lee[*,†]

[†]Powder and Ceramics Division, Korea Institute of Materials and Science, Changwondaero 797, Seongsan-gu, Changwon 51508, Korea

[‡]Department of Nano Energy Engineering, Pusan National University, Busandaehak-ro 63beon-gil 2, Geumjeong-gu, Busan 46241, Korea

[§]Department of Mechanical Engineering, Korea Advanced Institute of Science and Technology, Daehak-ro 291, Yuseong-gu, Daejeon 34141, Korea

[∥]Center for Environment, Health, and Welfare Research, Korea Institute of Science and Technology, Hwarang-ro 14-gil 5, Seongbuk-gu, Seoul 02792, Korea

Supporting Information

ABSTRACT: A highly stretchable, low-cost strain sensor was successfully prepared using an extremely cost-effective ionic liquid of ethylene glycol/sodium chloride. The hysteresis performance of the ionic-liquid-based sensor was able to be improved by introducing a wavy-shaped fluidic channel diminishing the hysteresis by the viscoelastic relaxation of elastomers. From the simulations on visco-hyperelastic behavior of the elastomeric channel, we demonstrated that the wavy structure can offer lower energy dissipation compared to a flat structure under a given deformation. The resistance response of the ionic-liquid-based wavy (ILBW) sensor was fairly deterministic with no hysteresis, and it was well-matched to the theoretically estimated curves. The ILBW sensors exhibited a low degree of hysteresis (0.15% at 250%), low overshoot (1.7% at 150% strain), and outstanding durability (3000 cycles at 300% strain). The ILBW sensor has excellent potential for use in precise and quantitative strain detections in various areas, such as human motion monitoring, healthcare, virtual reality, and smart clothes.

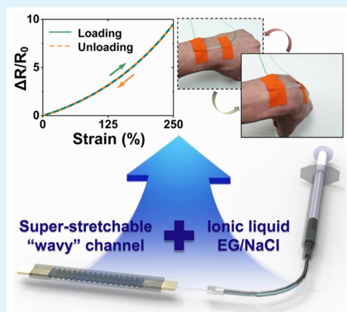

KEYWORDS: *stretchable sensor, strain sensor, human motion detection, ionic liquid, viscoelastic effect*

■ INTRODUCTION

A wearable strain sensor with skin-like sensing capability has diverse potential applications, such as human motion detection,[1−4] personal health monitoring,[5,6] prostheses,[7] smart clothes,[8] and soft robotics.[9] Conventional metal-foil strain gauges are ill-suited for these novel technologies, as they are merely able to detect relatively small strains of <5%.[10] Hence, numerous attempts have recently been made to realize a new conceptual strain sensor showing high stretchability and good sensitivity (i.e., gauge factor, GF) by engineering structures of conductive nanomaterials on elastic substrates.[11−13] For example, piezoresistive strain sensors based on a thin film of conducting nanomaterials, such as carbon nanotubes (CNTs),[1,3,5,14,15] carbon black particles,[16,17] graphene sheets,[4,18,19] silver nanowires (Ag NWs),[10,20] and metal nanoparticles,[21−24] have been introduced. They exhibited high performances in terms of the maximum strain, GF, and durability, but they also demonstrated significant overshoot and hysteresis. Because ubiquitous friction between solid-state conductors and elastomeric molecules leads to disparate time scales in detachment and slippage among the conductors,[10,14,17] large hysteresis was inevitably accompanied. The hysteretic behavior according to the strain history gives rise to significant errors in deformation measurements and should therefore be addressed so as to ensure precise and deterministic sensing capabilities. In this regard, sensors based on the piezocapacitance of a dielectric elastomer sandwiched between percolation networks of CNTs or Ag NWs have been proposed.[2,9,25,26] They displayed outstanding linearity and low hysteresis, but their theoretically limited GF of 1.0 is problematic in terms of sensitivity.

Recently, liquid-state conductors of carbon greases,[27] liquid metals,[20,28−30] and ionic liquids[29−35] have been suggested as an ideal platform for stretchable electronic applications because liquid intrinsically possesses limitless and instantaneous deformability. Carbon-conductive greases are inexpensive and environmentally friendly suspensions of carbon black particles, but they also result in large hysteresis owing to their viscoelastic characteristics and the retarded reaggregation between filler−filler bonds when in a relaxed state.[27,36] Liquid metals with a

Received: September 29, 2016
Accepted: December 20, 2016
Published: December 20, 2016

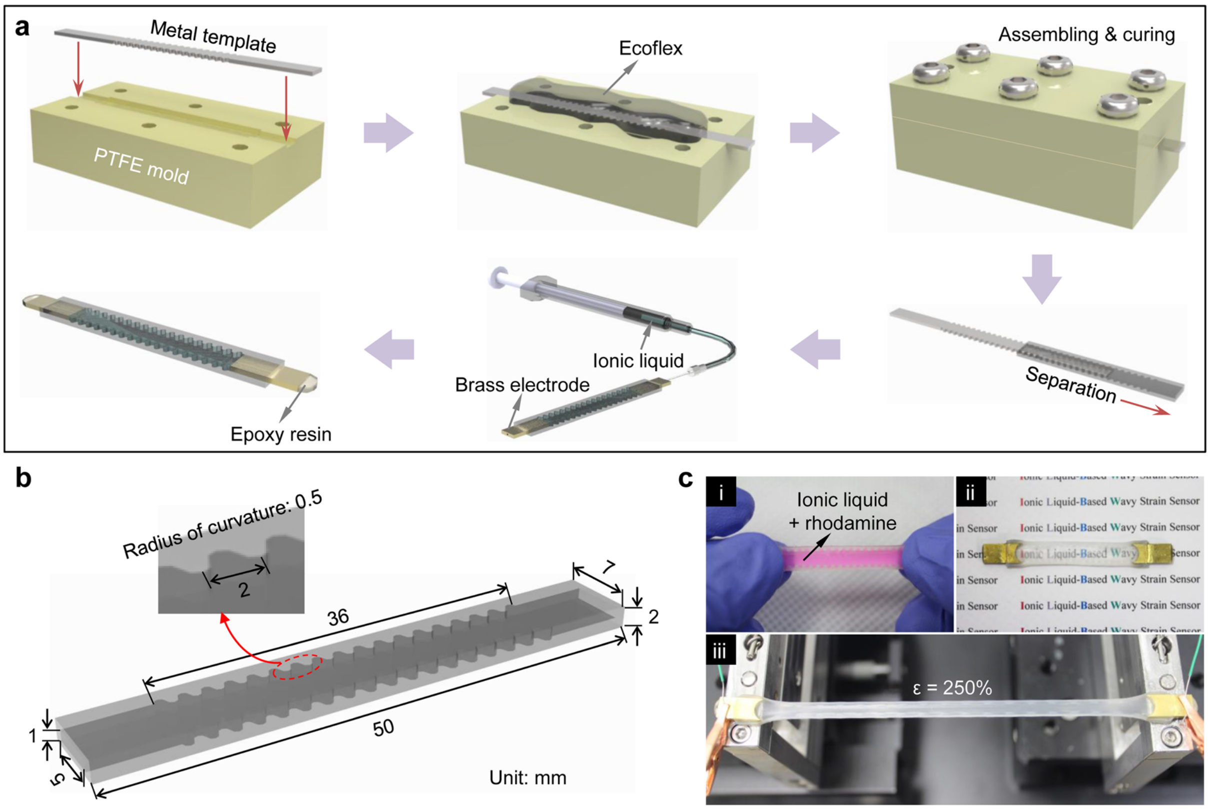

Figure 1. (a) Schematic illustration of the fabrication process of the ionic liquid-based strain sensor. (b) Geometrical dimensions of the ILBW strain sensor. (c) Photographs of the as-prepared ILBW strain sensor, indicating its (i) wavy structure, (ii) good transparency, and (iii) superstretchability.

good electrical conductivity ($3.4-3.5 \times 10^6$ S m^{-1}) are in the liquid state at room temperature, and they are utilized as a strain sensing element[28] or a liquid electrode[20,29,30] in stretchable sensor applications. However, their high cost would be an obstacle to those attempting to realize a low-cost stretchable sensor. Ionic liquids, defined as molten salts at ambient temperatures, have attracted much attention due to their several interesting characteristics such as nonvolatility, nonflammability, a high ion density, and high ionic conductivity.[37,38] Various ionic liquids have been successfully applied to fabricate microfluidics-based devices for sensing temperature, oxygen, pressure, and strain.[29−33] In spite of merits of liquid-state conductors such as mechanical deformability and electrical reversibility, the hysteretic response by the viscoelastic nature of elastomeric fluidic channels remains as a challenging task for simultaneously guaranteeing hysteresis-free and deterministic sensing capabilities even under a large strain. For precisely identifying introduced deformations, therefore, it is necessary to suppress the viscoelastic effect of the elastomeric substrate itself.[2,10]

Herein, we introduce a low-cost, superstretchable, and hysteresis-free strain sensor based on the ionic liquid of ethylene glycol (EG) and sodium chloride (NaCl) encapsulated within a symmetric wavy channel. The ionic liquid-based wavy (ILBW) sensors exhibited improved hysteresis performance compared to normal ionic liquid-based flat (ILBF) strain sensors. A simple model was proposed to explain the relationship between the viscoelasticity of elastomers and the hysteresis in electrical responses. Moreover, we verified that the wavy structure can produce lower energy dissipation compared to a flat structure under a given strain by conducting a finite element analysis (FEA) of visco-hyperelastic deformation of the elastomeric channel. The resistance response of the ILBW sensor was changed in a fairly deterministic manner, in good agreement with the theoretically predicted curve. The sensors also showed negligible hysteresis (0.15% at 250% strain), low overshoot (1.7% at 150% strain), and excellent durability (3000 cycles at 300% strain). These important features allow the ILBW sensor to be used for the reliable and quantitative detection of large strains, as was demonstrated by the motion monitoring of an index finger, elbow, and knee joint under various human activities.

EXPERIMENTAL METHODS

Fabrication of the Device. Both the top and bottom polytetrafluoroethylene (PTFE) molds were fabricated by conventional machining processes, and the metal template for the formation of the wavy channel (flat channel) was created through a laser cutting process with a stainless steel sheet. To fabricate a stretchable Ecoflex channel, part A and part B of the Ecoflex silicone elastomer (Ecoflex 00-50, Smooth-on) were mixed at a weight ratio of 1:1, vigorously stirred, degassed, and poured onto the metal template placed on the bottom PTFE mold, as shown in Figure 1a. The bottom PTFE mold was tightly combined with the top PTFE mold, and this set was then put into an electric oven preheated to 80 °C for 90 min to cure the Ecoflex. After curing, the Ecoflex was carefully separated from the metal template, and two brass electrodes with injection holes were bonded to the both ends of the Ecoflex channel using instant glue. The ionic liquid, a mixture of EG and NaCl (1.0 mol L^{-1}), was slowly injected through one of the holes of the brass electrodes using a syringe pump (LEGATO 180, kdScientific), after which the holes were sealed using epoxy glue.

Characterization of the Ionic Liquid. The viscosity of the ionic liquid was obtained from a rotational rheometer (HAAKE MARS, Thermo Scientific). The viscosity of the ionic liquid was 2.54×10^{-2} Pa s at 25 °C, which was slightly higher than that of EG (1.76×10^{-2}

DOI: 10.1021/acsami.6b12415
ACS Appl. Mater. Interfaces 2017, 9, 1770−1780

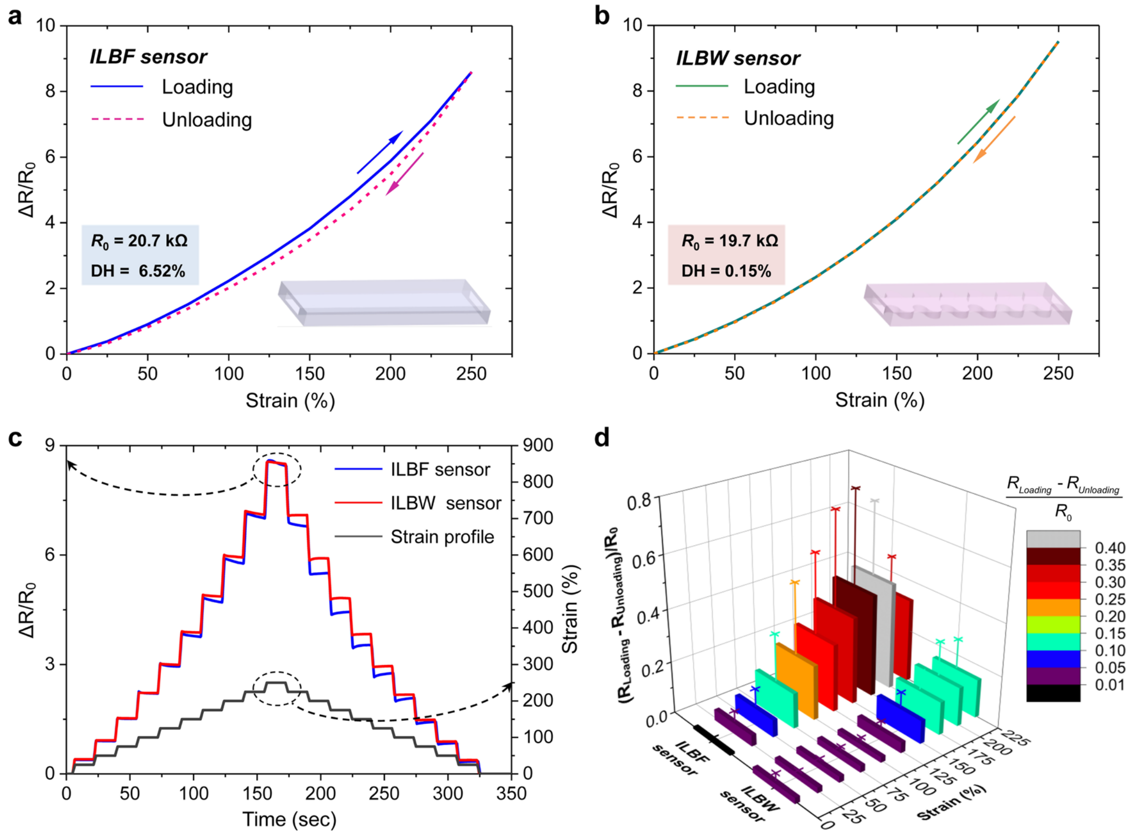

Figure 2. Comparison of the hysteresis performance between the ILBF and ILBW strain sensors. (a) Hysteresis curve of the ILBF strain sensor. The initial resistance (R_0) and the degree of hysteresis (DH) were 20.7 kΩ and 6.52%, respectively. (b) Hysteresis curve of the ILBW strain sensor. (R_0 = 19.7 kΩ; DH = 0.15%). (c) Plot of the relative change in the resistance of the ILBF and ILBW strain sensors under consecutive step-and-hold tests. (d) A 3D bar graph indicating the discrepancy in the resistance response between loading and unloading at each strain level. The height of each bar represents an average value obtained from several sample devices.

Pa). Measuring the electrical conductivity of the ionic liquid was performed with a conductivity meter (EC-40N, ISTEK Inc.). The electrical conductivity of pure EG was measured to be 5.12×10^{-5} S m^{-1}, and it was significantly increased to 2.72×10^{-1} S m^{-1} by the addition of 1 M NaCl.

Measurement of the Strain–Resistance Response. The prepared strain sensors were precisely stretched and released in a controlled manner using a programmable motion stage (SM1-0810-3S and STM-1-USB, Sciencetown) communicating with the computer. Before the tensile tests, the strain sensor was attached to the sample mounts of the motion stage system using instant glue, and copper wires were clamped to the brass electrodes to provide a connection to an external measurement device. The electrical resistance of the strain sensor was measured using a Keithley 2400 sourcemeter controlled by a computer through the LabView program. All of the strain-resistance characterization steps were conducted in an ambient environment, and unless especially noted, the strain rate was set to 10% s^{-1}.

Uniaxial Tensile and Stress Relaxation Tests. Tensile and relaxation test were conducted on dumbbell specimens of Ecoflex 00-50 using an Instron tensile testing machine with a 1 kN load cell. The test specimens with 3.3 mm thickness were produced by using a PTFE mold whose dimension is equal to that of the "dumbbell die A" as stated in ASTM standard D412-06a.[39] Ecoflex 00-50 was prepared by the same procedure used for the fabrication of the strain sensor. The top and bottom 20 mm parts of the specimen were clamped to sample holders and the specimen was then elongated at a crosshead speed of 500 mm min^{-1}. In the relaxation tests, the crosshead motion was stopped and the load was subsequently recorded as a function of time after the specimen was stretched to 300%. To determine the material constitutive parameters of the Ogden model and the Prony series model from the experimental data, the function "lsqcurvefit" in the Optimization Toolbox of MATLAB has been used.

Model Simulation. The finite element simulations were carried out using Abaqus/standard. Three-dimensional volume meshes for the flat channel and wavy channel were generated using 20-node quadratic brick (C3D20RH) and 10-node quadratic tetrahedral elements (C3D10H), respectively. Each channel was modeled using one-eighth symmetry to reduce the computational cost, and a uniaxial tensile boundary condition (strain rate = 10% s^{-1}) was applied.

In Vitro Cytotoxicity Tests of the Ionic Liquid. HeCaT human keratinocyte cells and HS68 human foreskin fibroblasts were purchased from the American Type Culture Collection (ATCC, U.S.A.), and the cells were stored in a 5% CO_2 humidified atmosphere at 37 °C. Dulbecco's Modified Eagle's Medium (DMEM; Hyclone, U.S.A.) was used for cell cultivation. These cells were supplemented with 10% (v/v) fetal bovine serum (FBS), 100 U/mL penicillin, and 100 μg/mL streptomycin. Cell viability upon exposure to EG, EG with 1 M NaCl, and soluble nickel compounds (SNCs; $NiSO_4$; Sigma-Aldrich) were examined using an EZ-Cytox cell viability assay kit (Daeil Lab Service Ltd., Korea) according to the manufacturer's instructions. Cells (1.5×10^4 cells/well) were plated in 96-well plates, incubated at 37 °C for 24 h, and given a fresh change of medium containing EG, EG with 1 M NaCl, and SNCs at the indicated concentration for 24 h. SNCs was used as reference control for cytotoxicity from environmental factors. At the end of the incubation, 10 μL of EZ-Cytox solution was added to the well and incubated for at least 1 more hour. The absorbance at 450 nm was measured using a Synergy HT Multimicroplate reader (BioTek Instruments, U.S.A.). Data were expressed as cell growth percentages relative to the control (no treatment) for each sample concentration.

DOI: 10.1021/acsami.6b12415
ACS Appl. Mater. Interfaces 2017, 9, 1770−1780

■ RESULTS AND DISCUSSION

Fabrication Scheme and Architecture of the ILBW Sensor. A simple casting technique was developed to fabricate the strain sensor consisting of a stretchable serpentine channel using a hyperelastic elastomer, Ecoflex 00-50, as shown in Figure 1a. Ecoflex is a platinum-catalyzed silicone rubber that can be stretched to more than 900% strain.[3] Its biocompatibility as well as its high mechanical compliance comparable to that of human skin are considered to make it highly applicable to epidermal electronic devices.[14] As shown in Figure 1a, liquid Ecoflex was strongly squeezed between a top PTFE mold and a bottom PTFE mold on which a wavy-patterned metal template was laid. After curing, the Ecoflex channel was carefully separated from the metal template. After conductive brass electrodes were bonded to both ends of the Ecoflex channel, a mixture of EG and NaCl, as a strain-sensitive element, was injected through small holes in the electrodes. Finally, two injection holes were sealed using epoxy resin. We selected EG instead of water as a dissociation medium for NaCl because it has a higher electrochemical stability window of ~4.0 V,[40] which is sufficiently beyond our operating voltage of 2.1 V; water generates bubbles of hydrogen and oxygen by electrolysis at voltages above ~1.23 V[41] and therefore offers a relatively narrow range of operating voltages. Moreover, the extremely low vapor pressure of EG is quite suitable for the long-term stability of devices (the vapor pressures of EG and water are ~0.01 kPa and ~3.17 kPa at 25 °C, respectively). In Table S1, prices of various active sensing materials used for wearable sensor applications are summarized. From the price comparison, it can be seen that the ionic liquid of EG-NaCl has superior cost-effectiveness compared with other materials, indicating great potential for utilization to low-cost wearable sensing devices.

Figure 1b presents the specific shape and dimensions of the ILBW strain sensor. Wavy structures whose waveforms are semicircular with radii of 0.5 mm were formed along the inner sidewalls of the channel. Figure 1c shows photographs of the as-prepared ILBW strain sensors, manifesting the wavy structure, optical transparency, and stretchability of the sensor. Rhodamine B dye was mixed with the ionic liquid to visualize the wavy structure of the elastomeric channel clearly, as shown in Figure 1c-i. It shows that the wavy patterns were successfully created along the inner sidewalls of the channel via the proposed facile casting method. The photograph presented in Figure 1c-ii reveals that the ILBW sensor was sufficiently transparent to observe the words vividly below the sensor. Figure 1c-iii shows a photograph of an ILBW sensor stretched to 250% strain, demonstrating its superstretchability.

Hysteresis Characteristics in Strain−Resistance Responses. To realize a strain sensor capable of detecting strains quantitatively and independently of the strain history, the electrical response of the sensor when stretched should be equal to that of the sensor when relaxed. That is, absence of hysteresis is crucial for a quantitative measurement of deformation by various dynamic stimuli commonly encountered in our everyday lives. By comparing the relative changes in the resistance, $(R/R_0) - 1$, during loading/unloading cycles, the hysteretic behaviors of the strain sensors were investigated. Figure 2a,b show the resistive responses of the ILBF sensor and the ILBW sensor, respectively. Each sensor was extended to 250% strain at a rate of 10% s^{-1} and relaxed back to the initial position at the same rate. As shown in Figure 2a, the ILBF sensor showed hysteretic behavior during the loading/unloading cycle. However, the ILBW sensor exhibited a negligible difference in the resistance responses between the loading and unloading curves, highlighting its hysteresis-free property and deterministic sensing performance (Figure 2b). We assessed the degree of hysteresis (DH) to quantitatively compare the hysteresis performances between them:[32]

$$\mathrm{DH} = \frac{A_{\mathrm{Loading}} - A_{\mathrm{Unloading}}}{A_{\mathrm{Loading}}} \times 100\% \tag{1}$$

where A_{Loading} and $A_{\mathrm{Unloading}}$ are the area of loading and unloading curves, respectively. A lower DH value indicates lesser hysteresis in the electrical response. The DH value of the ILBF sensor was about 6.52%. However, the ILBW sensor showed much smaller DH value of 0.15%, which was ~43.5 times smaller than that of the ILBF sensor. The strain-resistance responses of each sensor type prepared from different batches of Ecoflex also exhibited similar hysteresis characteristics to the above results (Figure S1). Regardless of the sidewall thickness of the channel, the ILBF sensors showed higher hysteresis in resistance−strain curve compared to the ILBW sensors. The hysteresis performance of the ILBW sensor was compared with that of previously reported wearable strain sensors and was found to be superior even under larger deformation (Table S2). We conducted step-and-hold tests to examine the resistance relaxation with time for each sensor, as shown in Figure 2c. At every step, the sensors were stretched by 25% with a strain rate of 10% s^{-1} and were held for 15 s. After being stretched to 250%, the sensors were released by 25% at the same rate and delay time. The resistance relaxation of the ILBW sensor was nearly negligible even under 250% strain, whereas that of the ILBF sensor increased with the strain. From these results, the hysteresis performance seems to be correlated very closely to the characteristic of resistance relaxation with time. The resistance relaxation behavior of the ILBF sensor was highly analogous to the stress relaxation behavior of viscoelastic materials; the stress decreases during the stress relaxation process when the material is stretched, while the stress increases when the material is released.[42,43] Hence, the improved hysteresis performance of the ILBW sensor is thought to have derived from the suppressed viscoelastic relaxation by the wavy structure of the elastomeric channel.

The discrepancy in the resistance responses between loading and unloading, $(R_{\mathrm{Loading}} - R_{\mathrm{Unloading}})/R_0$, was investigated for both ILBF sensor and ILBW sensor, as shown in the 3D bar graph in Figure 2d. The results for each sensor type were obtained from six test devices. The ILBF sensors showed a large discrepancy of ~21% at 100% strain; however, the ILBW sensors only showed a small value of ~2.1%. Furthermore, the discrepancy in the resistance responses of the ILBF sensors increased to ~41% at 200% strain, whereas that of the ILBW sensors was remained below 15%. Thus, the ILBW sensor is expected to provide more reliable and precise sensing capabilities than the ILBF sensor.

Figure S2a shows the strain-resistance curves of a single ILBW sensor under successive loading/unloading cycles. Although the hysteretic behavior of the sensor was notably aggravated by the pronounced viscoelastic effect of the elastomeric channel above 350% strain, the strain level of 250% guaranteeing negligible hysteresis sufficiently covers the detection range of human body motions. The sensor was functioned up to ~830% without failure owing to the limitless

DOI: 10.1021/acsami.6b12415
ACS Appl. Mater. Interfaces 2017, 9, 1770−1780

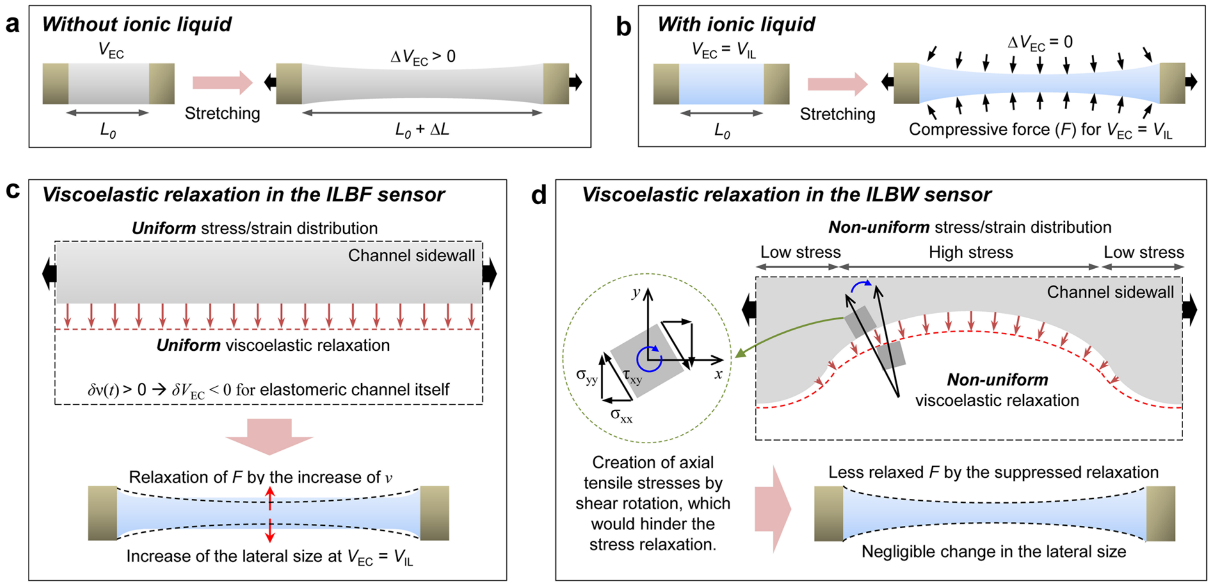

Figure 3. Difference in the viscoelastic relaxation process between the flat channel and wavy channel. (a) Elastomeric channel unfilled with the ionic liquid. The volume of the elastomeric channel (V_{EC}) is increased when the channel is stretched. (b) Elastomeric channel filled with the ionic liquid. V_{EC} is equal to that of ionic liquid (V_{IL}) regardless of deformation. (c) Schematic showing a segment of the stretched sidewall of the flat channel. The lateral length of the ILBF sensor can be increased resulted from the reduced compressive force (F) by the uniform viscoelastic relaxation. (d) Schematic showing a segment of the stretched sidewall of the wavy channel. To deform the curved surface, shear rotation should be involved owing to the unevenly distributed stress/strain. The introduced axial stress component of the shear stress acts to suppress the relaxation, and thus, the lateral length change of the ILBW sensor can be diminished.

deformability of the ionic liquid as well as the high-stretchability of Ecoflex itself (Figure S2b).

Relationship between Viscoelastic Relaxation and Resistance Hysteresis. The hysteresis performances of other stretchable strain sensors based on the percolation networks of solid-state conductors are affected by not only (i) stress relaxation caused by the viscoelasticity of the elastomer but also (ii) the imperfect recovery of conduction paths by the ubiquitous friction between the conductors and polymer molecules.[2,10,27] Because the second problem was circumvented by utilizing the ionic liquid, the viscoelastic effect of the elastomeric channel appears to act as a key factor causing the hysteresis of the ILBF sensor. We propose a simple mechanism for explaining the occurrence of the hysteresis in the electrical responses. The hysteresis in the resistance−strain diagram could be explained by the change in the lateral channel size resulted from the viscoelastic relaxation of the elastomeric channel. As the Poisson's ratios of elastomers are smaller than 0.5 in practice,[29] the volume of the elastomeric channel itself (V_{EC}) will be increased as it is elongated (Figure 3a). However, the volume of the channel filled with the ionic liquid will not change regardless of deformation due to the incompressibility of the ionic liquid. To satisfy the volume constraint ($V_{EC} = V_{IL}$), compressive forces (F) are exerted on the elastomeric channel to produce further contraction in the lateral direction, as shown in Figure 3b. Poisson's ratio (ν) of viscoelastic materials is a time-dependent material property. Because the shear modulus relaxes much more than the bulk modulus, the viscoelastic Poisson's ratio is a monotone increasing function of time, t ($d\nu/dt \geq 0$).[44,45] A constant Poisson's ratio is physically possible only for incompressible materials with $\nu(t) = 0.5$. However, such Poisson's ratio is highly restrictive condition for real materials.[45] During the stress relaxation process, the compressive force required for maintaining the constant channel volume is mitigated along with the increase of Poisson's ratio. For the flat channel, the viscoelastic relaxation would be equally produced by the uniform strain/stress distribution, as shown in Figure 3c. The lateral contraction is uniformly introduced by the weakened compressive force during the viscoelastic relaxation, and the channel width could be increased while maintaining the channel volume. Consequently, the resistance of the ILBF sensor is decreased with the viscoelastic relaxation. If the sidewalls of the elastomeric channel become serpentine, however, the stress relaxation would be unequally progressed due to the uneven strain/stress distribution (Figure 3d). The lateral contraction would also be nonuniformly introduced, and thus shear rotation is required to deform the curved surface of the wavy channel. Because the axial component of the shear stress acts to hinder the stress relaxation, the compressive force is less relaxed, and the change in lateral length could be reduced accordingly. Hence, the ILBW sensor could give a better hysteresis performance compared with the ILBF sensor.

Numerical Analysis of Visco-Hyperelastic Behavior. We performed a FEA to investigate the effect of the channel geometry on the hysteretic behavior of the sensor using the commercial FEA software Abaqus. A hyperelastic material model, the Ogden model, was used to take into account the nonlinear stress−strain characteristics of the Ecoflex 00-50 under large deformation. In the Ogden model, the strain energy potential function is expressed in terms of the principal stretches λ_i,[46]

$$U = \sum_{i=1}^{n} \frac{2\mu_i}{\alpha_i^2}(\lambda_1^{\alpha_i} + \lambda_2^{\alpha_i} + \lambda_3^{\alpha_i} - 3) \tag{2}$$

where μ_i, and α_i are the material coefficients. To acquire the Ogden material parameters of Ecoflex 00-50, we conducted uniaxial tensile tests using a dumbbell specimen as shown in Figure 4a. With the experimental data plotted in Figure 4b, a

DOI: 10.1021/acsami.6b12415
ACS Appl. Mater. Interfaces 2017, 9, 1770−1780

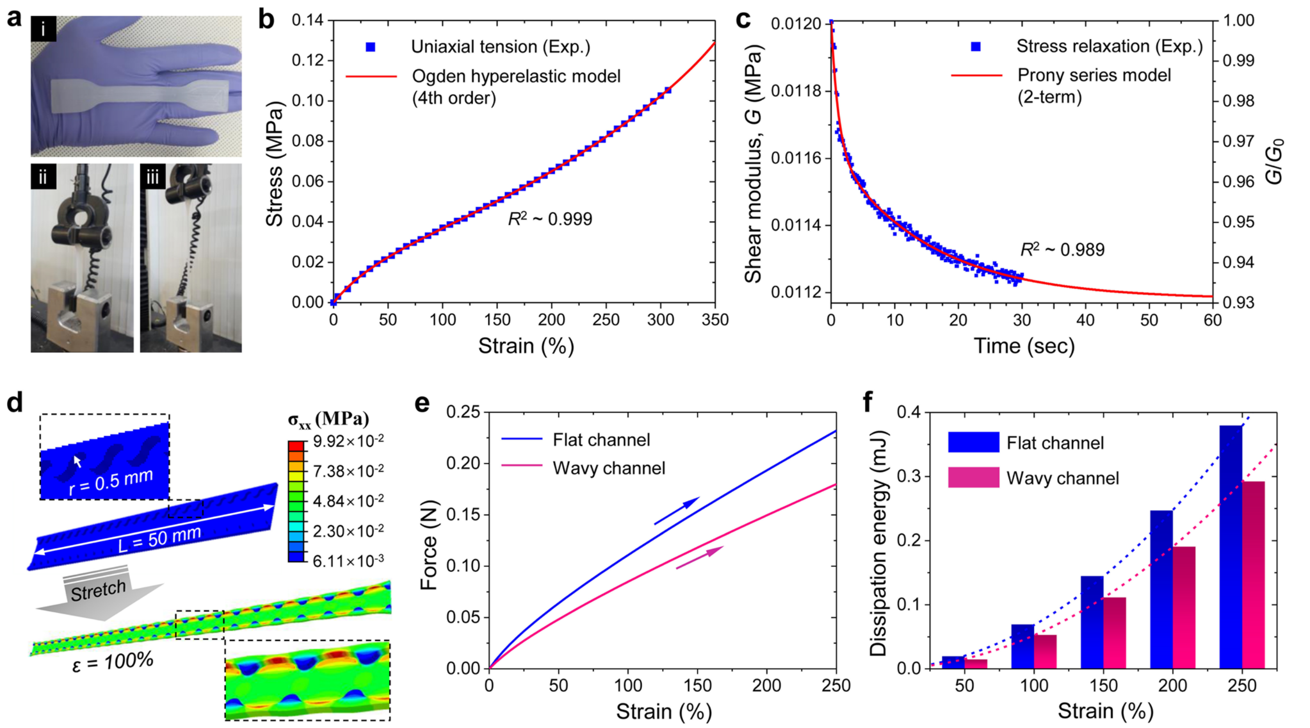

Figure 4. (a) Photographs of (i) dumbbell specimen made of Ecoflex 00-50 for tension and relaxation tests, (ii) undeformed specimen mounted on a material testing machine, (iii) specimen under a uniaxial tensile strain of 300%. (b) Stress−strain curve obtained by Ogden model fit to the data gathered from a uniaxial tensile testing. (c) Stress relaxation test results showing the decrease in shear modulus over time. The relaxation data was fitted to the 2-term Prony series model. (d) FEA model of the wavy channel (top) and contour plot of the longitudinal stress when stretched to 100% (bottom). (e) Simulated strain-force curves for the flat channel and wavy channel. (f) Dissipation energy according to the strain level for the flat channel and wavy channel.

least-squares fit of the stress−strain equations were computed to determine the parameters of the Ogden model.[47,48] The optimized parameters for the fourth order Ogden model are $\alpha_1 = 1.08$, $\alpha_2 = 13.99$, $\alpha_3 = -9.59$, $\alpha_4 = 4.49$, $\mu_1 = 2.08 \times 10^{-2}$ MPa, $\mu_2 = 2.14 \times 10^{-10}$ MPa, $\mu_3 = -6.01 \times 10^{-3}$ MPa, and $\mu_4 = 5.40 \times 10^{-3}$ MPa. The viscoelastic effect was included by considering the shear relaxation modulus $G(t)$ and the bulk relaxation modulus $K(t)$. Each relaxation modulus can be expressed based on the Prony series via the following equations:[49]

$$G(t) = G_0[1 - \sum_{i=1}^{n} g_i(1 - e^{-t/\tau_i})] \tag{3}$$

$$K(t) = K_0[1 - \sum_{i=1}^{n} k_i(1 - e^{-t/\tau_i})] \tag{4}$$

Here, G_0 and K_0 are the instantaneous shear modulus and bulk modulus, respectively, and g_i, k_i, and τ_i are the material coefficients. Usually, the bulk relaxation modulus is nearly invariant with respect to time for incompressible or nearly incompressible materials. Therefore, it can be neglected. Figure 4c represents the relaxation of the shear modulus of the Ecoflex 00-50 as a function of time, which was fitted using a 2-term Prony series model. It can be seen from the dimensionless shear modulus (G/G_0) that the relaxation is about 4.2% after a time of 5 s elapses. The Prony series coefficients were determined to be $G_0 = 1.201 \times 10^{-2}$ MPa, $g_1 = 3.18 \times 10^{-2}$, $g_2 = 3.722 \times 10^{-2}$, $\tau_1 = 1.141$ s, and $\tau_2 = 15.087$ s. The model of the wavy channel (a half-channel for the ILBW sensor) is depicted in the top image in Figure 4d. The length of the wavy channel is 50 mm, and the semicircular patterns with the radius of 0.5 mm were created along the sidewalls. Its average channel width and sidewall thickness are equal to those of the flat channel, as illustrated in Figure S3. When uniaxial strain of 100% was applied, the deformed shape of the wavy channel and the corresponding contour plot of the longitudinal stress (σ_{xx}) are shown in the bottom image in Figure 3d. In contrast to the uniform stress distribution in the flat channel, the stress is concentrated locally at the dimples (semicircular concave surfaces). Accordingly, the dimples are deformed more largely compared to the bumps (semicircular convex surfaces). As shown in Figure 4e, the required force to elongate the wavy channel by 250% is approximately 22.5% less than that for stretching the flat channel. These results show that the wavy channel provides better mechanical compliance compared to the flat channel; the higher compliance of the wavy channel is originated from the reduced equivalent stiffness by its wavy-shaped sidewalls. With the assumption of linear isotropic elasticity, we analytically calculated equivalent stiffness for each shape of the channel sidewall. The equivalent stiffness of the wavy structure is ∼17.3% lower than that of the flat structure (details in Supporting Information).

Figure 4f shows the simulation results of the dissipated energy by the viscoelastic effect of each channel during the first loading/unloading cycle. The dissipation energy increases nonlinearly according to the strain; however, interestingly, the dissipation energy in the wavy channel is lower compared to that of the flat channel at a given strain. The normalized difference in the dissipation energies (DE) between those of the flat channel and wavy channel, defined as $(DE_{flat} - DE_{wavy})/DE_{flat}$, was about 23.0% at 250% strain. Because the

DOI: 10.1021/acsami.6b12415
ACS Appl. Mater. Interfaces 2017, 9, 1770−1780

hysteresis loop area in stress−strain curves physically correlates with the degree of the dissipated energy during the loading−unloading cycle, the smaller dissipation energy means the lower hysteretic behavior. Thus, the calculated results shows that the wavy channel could give better hysteresis performance.

Quantitative Prediction of Resistance Response with Strain. For the strain sensor based on a liquid-state conductor, its resistance change is closely related to the geometrical changes in the length and cross-sectional area of the fluidic channel. Assuming the material is isotropic and incompressible, the relative change in the resistance can be expressed as[28]

$$\frac{\Delta R}{R_0} = \beta(\varepsilon^2 + 2\varepsilon) \tag{5}$$

where R_0 and ε is the measured initial resistance and the applied strain, respectively. The fitting parameter, β, accounts for the contact resistance between the electrode and the ionic liquid. A fit of eq 5 to the experimental data presented in Figure 5 gave a β = 0.797, with the corresponding coefficient of

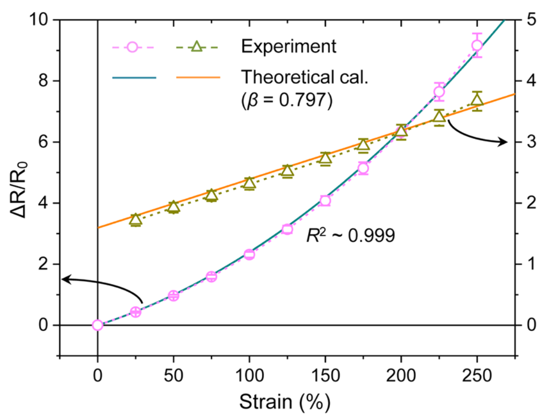

Figure 5. Plot of the relative change in the resistance and the gauge factor (GF) of the ILBW sensors as a function of the strain: the measured relative change in the resistance (circle), the measured GF (triangle), the calculated relative change in the resistance (cyan line), and the calculated GF (orange line).

determination (R^2) of ∼0.999. As is evident from Figure 5, the nonlinear change in the resistance of the ILBW sensor is well-explained by the above formula. The GF of the sensor can be calculated from the following definition; GF = $(\Delta R/R_0)\varepsilon^{-1}$ = $\beta(\varepsilon + 2)$. The predicted GF is in good agreement with the experimental result, and the GF linearly increased with the strain due to the quadratic feature of the electrical response of the sensor. As shown in Figure S5, the ILBF sensors, however, exhibited larger discrepancies between the measured and calculated data compared with the ILBW sensors, indicating that the ILBW sensors are able to offer more reliable and predictable sensing capabilities. In the derivation of eq 5, we only considered uniform deformation of the fluidic channel. Deformation of the cross-sectional area along the longitudinal direction could occur unevenly depending on the sensor geometry. Additionally, the nonuniform deformation could give rise to a different sensitivity from the above theoretical prediction.[34] For example, Yoon et al. demonstrated a highly sensitive ionic liquid-based transparent strain sensor with a GF = 40 at 200% strain.[32]

Dynamic Tensile Tests. To demonstrate deterministic sensing ability of the ILBW sensors, we conducted various dynamic loading tests, after which the experiment results were compared to the theoretically predicted resistance profile, as shown in Figure 6a,b. The dashed line represents the resistance profile estimated according to eq 5. In Figure 6a, the ILBW sensor was subjected to a tensile cyclic test with a triangular wave profile of which the peak strain values were progressively increased from 25% to 250%. The electrical resistance was promptly changed depending upon the applied strain without a noticeable delay within the resolution of our instruments (200 ms). In contrast to piezoresistive strain sensors composed of percolation networks of CNTs or Ag NWs,[9,10,15] the resistance response of the ILBW sensor was rarely affected by the strain history. The measured response corresponded closely to the calculated values. The mean and standard deviation values of $(\Delta R/R_0)_{\mathrm{calculated}}/(\Delta R/R_0)_{\mathrm{measured}}$ were 1.015 and 0.19, respectively, demonstrating the precise sensing ability of our sensors. Another sample device was mounted on the translation stage subjected to a series of "step-and-hold" motions, as shown in Figure 6b. The calculated resistance profile was well-matched with the experimentally obtained data. The ILBW sensor exhibited a low overshoot of ∼1.7% even at 150% strain, and its resistance response was quite reproducible.

In order to assess the long-term stability of the ILBW sensor, the devices were subjected to multiple loading/unloading cycles. Figure 6c shows the relative changes in the resistance of the ILBW sensor during 10 000 cycles at a peak strain of 100%. The resistance response of the sensor was markedly stable and regular while maintaining constant base resistance. In addition, the response curve was nearly unchanged after 5000 cycles at the maximum strain of 200%, as shown in Figure 6d. Even under the maximum strain of 300%, the response feature was rarely deteriorated after 3000 cycles, exhibiting the excellent durability of our strain sensor.

Human Motion Detection. To demonstrate the applicability of ILBW strain sensors in wearable/skin-mountable electronics, we used the sensors to detect the motion of index finger, elbow, and knee joints, as shown in Figure 7. Before the test of finger motion detections, we examined the sensitivity feature according to the contact quality of the sensor to skin (Figure S6). When a solid contact was not made, the response performance of the sensor was aggravated by slippage or delamination of the finger-mounted sensor from the skin, as shown in Figure S6b,c. Accordingly, the ILBW sensors were mounted on each joint by tightly wrapping adhesive bandages to the electrode parts of the sensors. The resistance response to the folding/unfolding movements of the index finger is illustrated in Figure 7a and Movie S1. The resistance of the finger-mounted sensor increased rapidly upon the folding of the finger, regaining its original value once the finger was entirely relaxed. In addition, when the finger was held folded, the resistance was stably maintained without incurring significant relaxation. The maximum strain introduced by the folding of the index finger was estimated to be about 52%, which was similar to the previously reported results (35% − 45%).[4,14,26,50]

The sensing performance of the ILBW sensor was compared with that of a commercial strain sensor (FLK-1-11, Tokyo Sokki Kenkyujo Co., Ltd.) with a GF of 2.16. The small feature size of the commercial sensor was highly unsuitable to apply in the motion detection of human joints, and also, its polyimide support was too rigid to accompany the deformation introduced by finger skin. Consequently, even though the GF of the commercial sensor was similar to that of our sensor, the relative change in the resistance of the commercial sensor was

DOI: 10.1021/acsami.6b12415
ACS Appl. Mater. Interfaces 2017, 9, 1770−1780

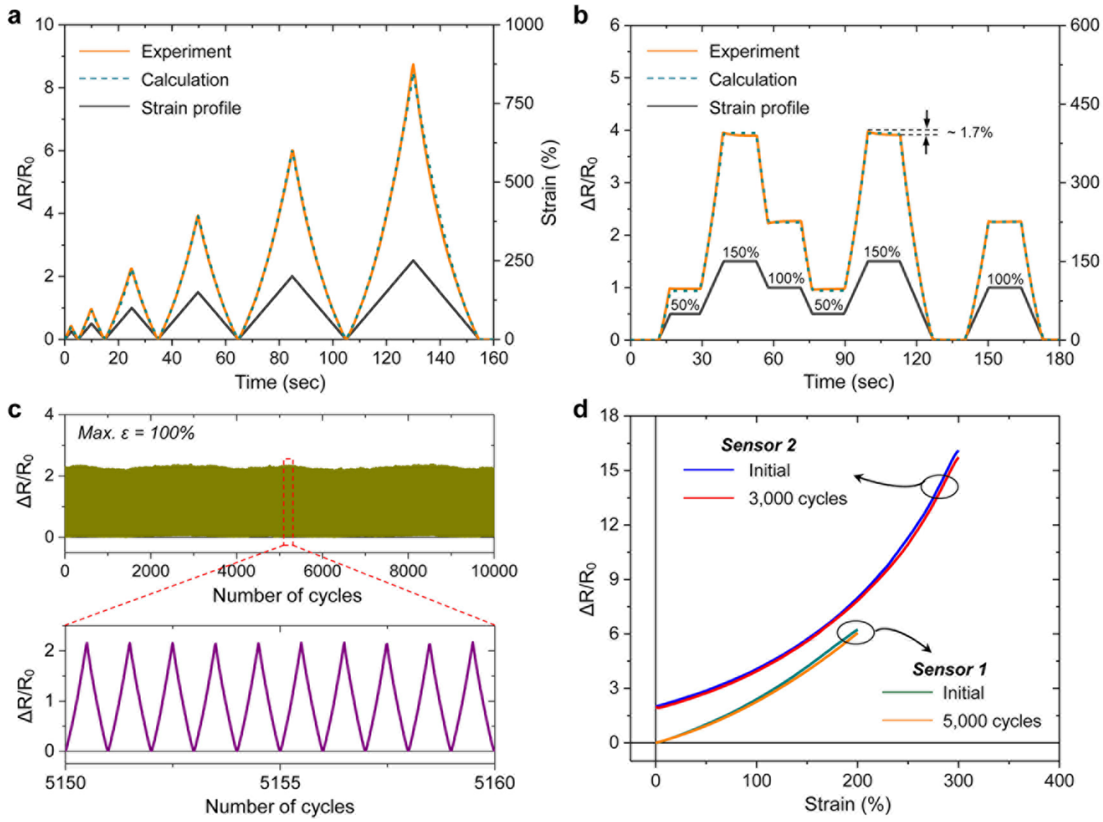

Figure 6. Various dynamic loading tests for the ILBW strain sensor. (a) Relative change in the resistance under a triangular strain profile. The magnitudes of the respective peak strains are 25, 50, 100, 150, 200, and 250%. (b) Relative change in the resistance under a trapezoidal strain profile. The delay time was set to 15 s. (c) Plot of the resistance response over 10 000 loading/unloading cycles at a maximum strain of 100% (top). The bottom plot for the region indicated by the red box shows the very stable and reproducible response of the ILBW sensor during the cyclic test. (d) Relative change in the resistance versus the strain after multiple loading/unloading cycles at strain of 0−200% (sensor 1) and 0−300% (sensor 2). The baseline for sensor 2 is shifted to 2.0.

>1000 times lower than that of the ILBW sensor, as shown in Figure 7b. More importantly, the commercial sensor showed substantial overshoots and undershoots during the folding/unfolding movements of the index finger.

Figure 7c shows the changes in resistance signals of the finger-mounted ILBW sensor according to the actions of gripping various bottles with a single hand. As curvature of the bottle increased, the index finger is more bent and the resistance of the sensor was also raised accordingly.

Figure 7d presents the sensing performance of the ILBW sensor attached to the elbow joint. The elbow-mounted sensor reliably detected resistance changes depending on the degree of the bending of the elbow joint, and the sensor distinguishably responded to different elbow motions (Movie S2). The resistance was increased simultaneously with the bending of the elbow, and remained nearly unchanged while the elbow was kept flexed. The maximum strain produced by the full bending of the elbow was estimated to be approximately 70%.

We also measured the motion of the knee in real time during various activities of flexing, squatting, jumping and marching, as shown in Figure 7e. The resistance of the knee-mounted sensor in a standing posture was increased by the knee flexion and remained mostly constant as long as the knee was kept flexed. When the wearer squatted down, the skin around the knee joint was additionally stretched; consequently, the resistance was further increased. While maintaining the squatting posture, the resistance was nearly unchanged. The complex motion of jumping can be distinctly identified by the first rapid rise in the resistance resulted from the knee flexion prior to the jump, by the sharp drop in the resistance resulted from the knee extension when the wearer jumped, by the second rapid rise in the resistance resulted from the slight flexure of the knee when the wearer landed, and by the drop in the resistance to its initial value when the wearer returned to the standing position. While the wearer was marching, the knee-mounted sensor exhibited a repetitive increase and decrease of the resistance by the consecutive flexion and extension of the knee joint.

Biocompatibility Tests of the Ionic Liquid. Along with the sensor performance, the biocompatibility of the sensing material is also important for real application of wearable strain sensors. Even though the test devices were not damaged during the motion monitoring of various human joints (Figure S7), leakage of the ionic liquid by accidental damage of the device would cause skin injuries if the ionic liquid is toxic for human skins. Therefore, it is necessary to conduct studies on the biocompatibility of the ionic liquid to assess whether it can used as a sensing component of human-friendly wearable sensors. In order to evaluate the toxicity of the ionic liquid (a mixture of EG and 1 M NaCl), in vitro cytotoxicity tests were performed using HeCaT human keratinocyte cells and HS68 human foreskin fibroblasts, the results of which were compared with those of SNCs causing genotoxic effects in cells.[51] The SNCs are classified as a human carcinogen by the U.S. National Toxicology Program (NTP) and Beraterkreis Toxikologie in Germany; however, it is a weaker carcinogen than other insoluble nickel compounds.[52] Figure 8 shows the cell viability

DOI: 10.1021/acsami.6b12415
ACS Appl. Mater. Interfaces 2017, 9, 1770−1780

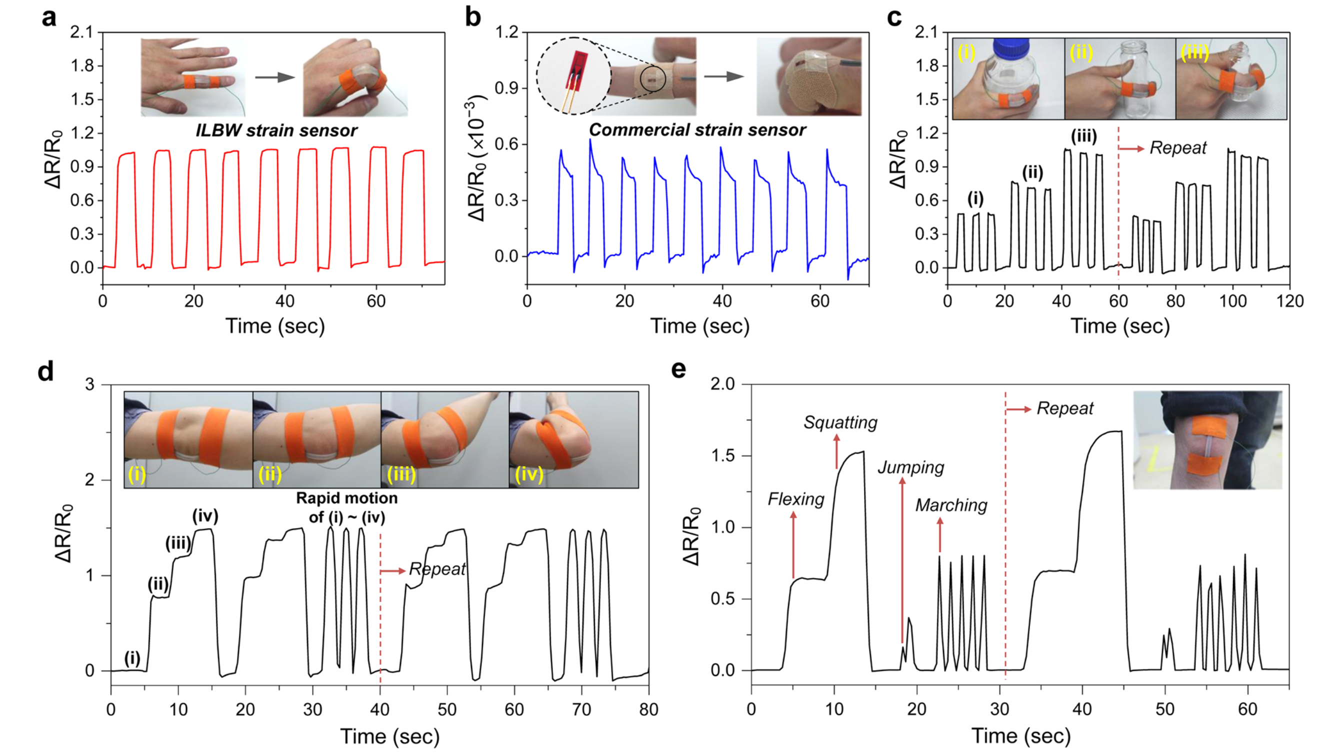

Figure 7. Monitoring of various human joint motions in real time. (a,b) Electrical resistance responses for folding/unfolding motions of an index finger equipped with (a) the ILBW sensor (R_0 = ∼ 17.8 kΩ) and (b) a commercial sensor (R_0 = ∼ 121.1 Ω). (c) Relative change in the resistance of the ILBW sensor at single-handed gripping of bottles with different sizes: (i) diameter (d) = 102 mm; (ii) d = 42 mm; (iii) d = 26 mm. (d,e) Relative change in the resistance of the ILBW sensor at (d) various bending states of an elbow joint and (e) at the various movements of a knee joint.

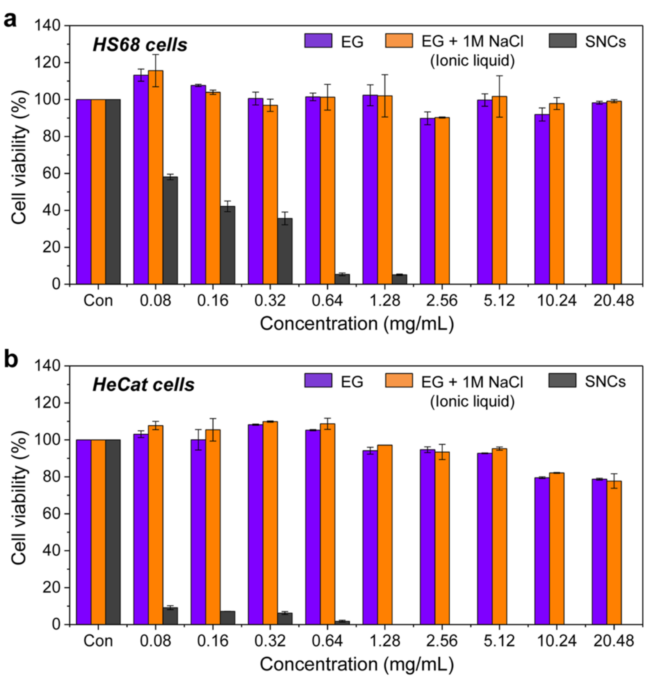

Figure 8. Cytotoxicity tests of the ionic liquid. The cell viability (%) of (a) HS68 cells and (b) HeCat cells depending on the concentration of EG, EG with 1 M NaCl (ionic liquid), and a SNCs. Error bars indicate standard deviations.

depending on various concentrations of pure EG, the ionic liquid, and the SNC on HS68 and HeCaT cells. The concentration of SNCs needed to reach 50% inhibition of the test cells (IC50) following 24h exposures was ∼0.16 mg/mL on HS68 cells and <0.08 mg/mL on HeCaT cells, respectively. For both cell types, however, EG and the ionic liquid show negligible cell toxicity comparing to the SNC even at a relatively high concentration of 20.48 mg/mL. These results corresponded that the IC50 of EG or the ionic liquid is much higher than 20.48 mg/mL. Although the in vitro tests showed that the ionic liquid is much less toxic than the carcinogen, it does not mean that the ionic liquid is harmless to human skins. Thus, in vivo experiments are additionally required, and this will be an important subject of a future investigation.

CONCLUSIONS

A highly stretchable, low-cost, and hysteresis-free strain sensor was achieved by introducing the ionic liquid of EG/NaCl and a wavy-shaped hyperelastic channel. The trade-off relationship between the stretchability and sensing precision by the hysteresis according to the strain history were able to be overcome through the combination of the limitless deformability of liquid and the less hysteretic wavy structure of the fluidic channel. We developed a simple model to describe the relationship between viscoelasticity of the elastomers and the hysteresis in the electrical response. From the simulations on visco-hyperelastic behavior of the elastomeric channel, the wavy structure was found to offer lower energy dissipation compared to a flat structure under a given deformation. Accordingly, the hysteresis performance of the ILBW sensor was superior to that of the ILBF sensor. The resistance response of the ILBW sensor was fairly deterministic and theoretically predictable. Moreover, the ILBW sensors showed outstanding durability, low overshoot, and ultrastretchability. These excellent performance capabilities make the ILBW sensor applicable for precise and quantitative strain sensing in various wearable electronic

DOI: 10.1021/acsami.6b12415
ACS Appl. Mater. Interfaces 2017, 9, 1770−1780

applications, such as human motion detection, personal health monitoring, virtual reality, and smart clothing systems.

■ ASSOCIATED CONTENT

Supporting Information

The Supporting Information is available free of charge on the ACS Publications website at DOI: 10.1021/acsami.6b12415.

Price comparison of active sensing materials applied to wearable strain sensors, degree of hysteresis for various types of wearable strain sensors, hysteresis in the strain-resistance response of the ILBF sensors and ILBW sensors, hysteretic behavior of the ILBW sensor under successive loading/unloading cycles, FEA results for the flat channel, effective stiffness of the sidewalls of the wavy channel and the flat channel, the relative change in the resistance and the GF of the ILBF sensors, sensitivity performance depending on the quality of contact, and examination of leakage of the ionic liquid (PDF)

Movie S1: resistance response to the folding/unfolding movements of the index finger (AVI)

Movie S2: resistance response to the degree of elbow bending and different elbow motions (AVI)

■ AUTHOR INFORMATION

Corresponding Authors

*E-mail for H.M.L.: hyelee@kims.re.kr.

*E-mail for H.W.L.: LHW2010@pusan.ac.kr.

ORCID

Hyung Jin Sung: 0000-0002-4671-3626

Hye Moon Lee: 0000-0001-6719-5613

Author Contributions

¶D.Y.C. and M.H.K. contributed equally to this work.

Notes

The authors declare no competing financial interest.

■ ACKNOWLEDGMENTS

This study was supported financially by the Fundamental Research Program (PNK4661) of Korea Institute of Materials Science (KIMS) and by the Civil & Military Technology Cooperation Program through the National Research Foundation of Korea (NRF) (No.2013M3C1A9055407) funded by Ministry of Science, ICT & Future Planning. This study was also partially supported by the KIST Institutional Program.

■ REFERENCES

(1) Yamada, T.; Hayamizu, Y.; Yamamoto, Y.; Yomogida, Y.; Izadi-Najafabadi, A.; Futaba, D. N.; Hata, K. A Stretchable Carbon Nanotube Strain Sensor for Human-Motion Detection. *Nat. Nanotechnol.* **2011**, *6*, 296−301.

(2) Cai, L.; Song, L.; Luan, P.; Zhang, Q.; Zhang, N.; Gao, Q.; Zhao, D.; Zhang, X.; Tu, M.; Yang, F.; et al. Super-Stretchable, Transparent Carbon Nanotube-Based Capacitive Strain Sensors for Human Motion Detection. *Sci. Rep.* **2013**, *3*, 3048.

(3) Ryu, S.; Lee, P.; Chou, J. B.; Xu, R.; Zhao, R.; Hart, A. J.; Kim, S.-G. Extremely Elastic Wearable Carbon Nanotube Fiber Strain Sensor for Monitoring of Human Motion. *ACS Nano* **2015**, *9*, 5929−5936.

(4) Yan, C.; Wang, J.; Kang, W.; Cui, M.; Wang, X.; Foo, C. Y.; Chee, K. J.; Lee, P. S. Highly Stretchable Piezoresistive Graphene−Nanocellulose Nanopaper for Strain Sensors. *Adv. Mater.* **2014**, *26*, 2022−2027.

(5) Roh, E.; Hwang, B.-U.; Kim, D.; Kim, B.-Y.; Lee, N.-E. Stretchable, Transparent, Ultrasensitive, and Patchable Strain Sensor for Human−Machine Interfaces Comprising a Nanohybrid of Carbon Nanotubes and Conductive Elastomers. *ACS Nano* **2015**, *9*, 6252−6261.

(6) Boland, C. S.; Khan, U.; Backes, C.; O'Neill, A.; McCauley, J.; Duane, S.; Shanker, R.; Liu, Y.; Jurewicz, I.; Dalton, A. B.; Coleman, J. N. Sensitive, High-Strain, High-Rate Bodily Motion Sensors Based on Graphene−Rubber Composites. *ACS Nano* **2014**, *8*, 8819−8830.

(7) Kim, J.; Lee, M.; Shim, H. J.; Ghaffari, R.; Cho, H. R.; Son, D.; Jung, Y. H.; Soh, M.; Choi, C.; Jung, S.; Chu, K.; Jeon, D.; Lee, S.-T.; Kim, J. H.; Choi, S. H.; Hyeon, T.; Kim, D.-H. Stretchable Silicon Nanoribbon Electronics for Skin Prosthesis. *Nat. Commun.* **2014**, *5*, 5747.

(8) Park, J. J.; Hyun, W. J.; Mun, S. C.; Park, Y. T.; Park, O. O. Highly Stretchable and Wearable Graphene Strain Sensors with Controllable Sensitivity for Human Motion Monitoring. *ACS Appl. Mater. Interfaces* **2015**, *7*, 6317−6324.

(9) Cohen, D. J.; Mitra, D.; Peterson, K.; Maharbiz, M. M. A Highly Elastic, Capacitive Strain Gauge Based on Percolating Nanotube Networks. *Nano Lett.* **2012**, *12*, 1821−1825.

(10) Amjadi, M.; Pichitpajongkit, A.; Lee, S.; Ryu, S.; Park, I. Highly Stretchable and Sensitive Strain Sensor Based on Silver Nanowire−Elastomer Nanocomposite. *ACS Nano* **2014**, *8*, 5154−5163.

(11) Rogers, J. A.; Someya, T.; Huang, Y. Materials and Mechanics for Stretchable Electronics. *Science* **2010**, *327*, 1603−1607.

(12) Hammock, M. L.; Chortos, A.; Tee, B. C. K.; Tok, J. B. H.; Bao, Z. 25th Anniversary Article: The Evolution of Electronic Skin (E-Skin): A Brief History, Design Considerations, and Recent Progress. *Adv. Mater.* **2013**, *25*, 5997−6038.

(13) Yao, S.; Zhu, Y. Nanomaterial-Enabled Stretchable Conductors: Strategies, Materials and Devices. *Adv. Mater.* **2015**, *27*, 1480−1511.

(14) Amjadi, M.; Yoon, Y. J.; Park, I. Ultra-Stretchable and Skin-Mountable Strain Sensors Using Carbon Nanotubes-Ecoflex Nanocomposites. *Nanotechnology* **2015**, *26*, 375501.

(15) Lipomi, D. J.; Vosgueritchian, M.; Tee, B. C.; Hellstrom, S. L.; Lee, J. A.; Fox, C. H.; Bao, Z. Skin-Like Pressure and Strain Sensors Based on Transparent Elastic Films of Carbon Nanotubes. *Nat. Nanotechnol.* **2011**, *6*, 788−792.

(16) Lu, N.; Lu, C.; Yang, S.; Rogers, J. Highly Sensitive Skin-Mountable Strain Gauges Based Entirely on Elastomers. *Adv. Funct. Mater.* **2012**, *22*, 4044−4050.

(17) Kong, J.-H.; Jang, N.-S.; Kim, S.-H.; Kim, J.-M. Simple and Rapid Micropatterning of Conductive Carbon Composites and Its Application to Elastic Strain Sensors. *Carbon* **2014**, *77*, 199−207.

(18) Wang, Y.; Yang, R.; Shi, Z.; Zhang, L.; Shi, D.; Wang, E.; Zhang, G. Super-Elastic Graphene Ripples for Flexible Strain Sensors. *ACS Nano* **2011**, *5*, 3645−3650.

(19) Li, X.; Zhang, R.; Yu, W.; Wang, K.; Wei, J.; Wu, D.; Cao, A.; Li, Z.; Cheng, Y.; Zheng, Q.; et al. Stretchable and Highly Sensitive Graphene-on-Polymer Strain Sensors. *Sci. Rep.* **2012**, *2*, 870.

(20) Kim, K. K.; Hong, S.; Cho, H. M.; Lee, J.; Suh, Y. D.; Ham, J.; Ko, S. H. Highly Sensitive and Stretchable Multidimensional Strain Sensor with Prestrained Anisotropic Metal Nanowire Percolation Networks. *Nano Lett.* **2015**, *15*, 5240−5247.

(21) Herrmann, J.; Müller, K.-H.; Reda, T.; Baxter, G.; Raguse, B.; De Groot, G.; Chai, R.; Roberts, M.; Wieczorek, L. Nanoparticle Films as Sensitive Strain Gauges. *Appl. Phys. Lett.* **2007**, *91*, 183105.

(22) Farcau, C.; Sangeetha, N. M.; Moreira, H.; Viallet, B. t.; Grisolia, J.; Ciuculescu-Pradines, D.; Ressier, L. High-Sensitivity Strain Gauge Based on a Single Wire of Gold Nanoparticles Fabricated by Stop-and-Go Convective Self-Assembly. *ACS Nano* **2011**, *5*, 7137−7143.

(23) Tanner, J.; Mousadakos, D.; Giannakopoulos, K.; Skotadis, E.; Tsoukalas, D. High Strain Sensitivity Controlled by the Surface Density of Platinum Nanoparticles. *Nanotechnology* **2012**, *23*, 285501.

(24) Lee, J.; Kim, S.; Lee, J.; Yang, D.; Park, B. C.; Ryu, S.; Park, I. A Stretchable Strain Sensor Based on a Metal Nanoparticle Thin Film for Human Motion Detection. *Nanoscale* **2014**, *6*, 11932−11939.

(25) Amjadi, M.; Park, I. Sensitive and Stable Strain Sensors Based on the Wavy Structured Electrodes, *Proceedings of the 14th International Conference on Nanotechnology*, IEEE-NANO, Toronto, Canada, August 18−21,2014; pp 760−763.

(26) Yao, S.; Zhu, Y. Wearable Multifunctional Sensors Using Printed Stretchable Conductors Made of Silver Nanowires. *Nanoscale* **2014**, *6*, 2345−2352.
(27) Muth, J. T.; Vogt, D. M.; Truby, R. L.; Mengüç, Y.; Kolesky, D. B.; Wood, R. J.; Lewis, J. A. Embedded 3d Printing of Strain Sensors within Highly Stretchable Elastomers. *Adv. Mater.* **2014**, *26*, 6307−6312.
(28) Matsuzaki, R.; Tabayashi, K. Highly Stretchable, Global, and Distributed Local Strain Sensing Line Using Gainsn Electrodes for Wearable Electronics. *Adv. Funct. Mater.* **2015**, *25*, 3806−3813.
(29) Chossat, J.-B.; Park, Y.-L.; Wood, R. J.; Duchaine, V. A Soft Strain Sensor Based on Ionic and Metal Liquids. *IEEE Sens. J.* **2013**, *13*, 3405−3414.
(30) Ota, H.; Chen, K.; Lin, Y.; Kiriya, D.; Shiraki, H.; Yu, Z.; Ha, T.-J.; Javey, A. Highly Deformable Liquid-State Heterojunction Sensors. *Nat. Commun.* **2014**, *5*, 5032.
(31) Cheung, Y.-N.; Zhu, Y.; Cheng, C.-H.; Chao, C.; Leung, W. W.-F. A Novel Fluidic Strain Sensor for Large Strain Measurement. *Sens. Actuators, A* **2008**, *147*, 401−408.
(32) Yoon, S. G.; Koo, H.-J.; Chang, S. T. Highly Stretchable and Transparent Microfluidic Strain Sensors for Monitoring Human Body Motions. *ACS Appl. Mater. Interfaces* **2015**, *7*, 27562−27570.
(33) Russo, S.; Ranzani, T.; Liu, H.; Nefti-Meziani, S.; Althoefer, K.; Menciassi, A. Soft and Stretchable Sensor Using Biocompatible Electrodes and Liquid for Medical Applications. *Soft Robot.* **2015**, *2*, 146−154.
(34) Wang, Y.; Gong, S.; Wang, S. J.; Simon, G. P.; Cheng, W. Volume-Invariant Ionic Liquid Microbands as Highly Durable Wearable Biomedical Sensors. *Mater. Horiz.* **2016**, *3*, 208−213.
(35) Zhu, Y.; Chao, C.; Cheng, C.-H.; Leung, W. W.-F. A Novel Ionic-Liquid Strain Sensor for Large-Strain Applications. *IEEE Electron Device Lett.* **2009**, *30*, 337−339.
(36) Stübler, N.; Fritzsche, J.; Klüppel, M. Mechanical and Electrical Analysis of Carbon Black Networking in Elastomers under Strain. *Polym. Eng. Sci.* **2011**, *51*, 1206−1217.
(37) Ohno, H.; Yoshizawa, M.; Ogihara, W. Development of New Class of Ion Conductive Polymers Based on Ionic Liquids. *Electrochim. Acta* **2004**, *50*, 255−261.
(38) Johnson, K. E. What's an Ionic Liquid? *Interface-Electrochemical Society* **2007**, *16*, 38−41.
(39) ASTM International. *Standard Test Methods for Vulcanized Rubber and Thermoplastic Rubbers and Thermoplastic Elastomers-Tension [D 412−06a]*; ASTM International: Conshohocken, PA, 2013.
(40) Lee, J.-W.; Koo, C. M. Ionic Electroactive Polymer Actuators. *Polymer Science and Technology* **2013**, *24*, 177−182.
(41) Zoulias, E.; Varkaraki, E.; Lymberopoulos, N.; Christodoulou, C. N.; Karagiorgis, G. N. A Review on Water Electrolysis. *TCJST* **2004**, *4*, 41−71.
(42) Bergström, J. S.; Boyce, M. C. Constitutive Modeling of the Large Strain Time-Dependent Behavior of Elastomers. *J. Mech. Phys. Solids* **1998**, *46*, 931−954.
(43) Lakes, R. S. *Viscoelastic Materials*; Cambridge University Press: New York, 2009;.
(44) Tschoegl, N. W.; Knauss, W. G.; Emri, I. Poisson's Ratio in Linear Viscoelasticity−a Critical Review. *Mech. Time-Depend. Mater.* **2002**, *6*, 3−51.
(45) Hilton, H. H.; Yi, S. The Significance of (an) Isotropic Viscoelastic Poisson Ratio Stress and Time Dependencies. *Int. J. Solids Struct.* **1998**, *35*, 3081−3095.
(46) Elsayed, Y.; Vincensi, A.; Lekakou, C.; Geng, T.; Saaj, C.; Ranzani, T.; Cianchetti, M.; Menciassi, A. Finite Element Analysis and Design Optimization of a Pneumatically Actuating Silicone Module for Robotic Surgery Applications. *Soft Robot.* **2014**, *1*, 255−262.
(47) Ogden, R.; Saccomandi, G.; Sgura, I. Fitting Hyperelastic Models to Experimental Data. *Comput. Mech.* **2004**, *34*, 484−502.
(48) Berselli, G.; Vassura, G.; Pellicciari, M.; Vertechy, R. *Hyperelastic Modeling of Rubber-Like Photopolymers for Additive Manufacturing Processes*; INTECH Open Access Publisher: Rijeka, Croatia, 2011.
(49) Moseley, P.; Florez, J. M.; Sonar, H. A.; Agarwal, G.; Curtin, W.; Paik, J. Modeling, Design, and Development of Soft Pneumatic Actuators with Finite Element Method. *Adv. Eng. Mater.* **2016**, *18*, 978−988.
(50) Luo, S.; Liu, T. Swcnt/Graphite Nanoplatelet Hybrid Thin Films for Self-Temperature-Compensated, Highly Sensitive, and Extensible Piezoresistive Sensors. *Adv. Mater.* **2013**, *25*, 5650−5657.
(51) Hwang, G. B.; Heo, K. J.; Yun, J. H.; Lee, J. E.; Lee, H. J.; Nho, C. W.; Bae, G.-N.; Jung, J. H. Antimicrobial Air Filters Using Natural Euscaphis Japonica Nanoparticles. *PLoS One* **2015**, *10*, 0126481.
(52) Oller, A. R. Respiratory Carcinogenicity Assessment of Soluble Nickel Compounds. *Environ. Health Perspect.* **2002**, *110*, 841−844.

DOI: 10.1021/acsami.6b12415
ACS Appl. Mater. Interfaces 2017, 9, 1770−1780